Electronic Supplementary Material (ESI) for Journal of Materials Chemistry A.
This journal is © The Royal Society of Chemistry 2020

Supporting Information

Alloy-Strain-Output Induced Lattice Dislocation in Ni_3FeN/Ni_3Fe Ultrathin Nanosheets for Highly Efficient Overall Water Splitting

Zijian Li,[a, d#] Haeseong Jang,[b#] Danni Qin,[a] Xiaoli Jiang,[a] Xuqiang Ji,[a,c*]
Min Gyu Kim,[d] Lijie Zhang,[a*] Xien Liu,[a*] and Jaephil Cho[b*]

a. *State Key Laboratory Base of Eco-Chemical Engineering, College of Chemical Engineering, Qingdao University of Science and Technology, Qingdao 266042 (China).*
b. *Department of Energy Engineering, School of Energy and Chemical Engineering, Ulsan National Institute of Science and Technology (UNIST), Ulsan 689-798 (South Korea).*
c. *College of Materials Science and Engineering, Qingdao University, Qingdao 266071, China*
d. *Department of Chemistry, City University of Hong Kong, Hong Kong, China*
e. *Beamline Research Division, Pohang Accelerator Laboratory (PAL), Pohang 790-784 (Korea).*

List of contents

Fig. S11 Cyclic voltammetry curves of the (a) d-Ni_3FeN/Ni_3Fe, (b) Ni_3Fe, (c) Ni_3FeN and (d) Ni_3FeN/Ni_3Fe-bulk at various scan rates (40, 60, 80 ,100 and 120 mV s^{-1}) in 1.0 M KOH for OER.

Fig. S12 Cyclic voltammetry curves of the (a) d-Ni_3FeN/Ni_3Fe, (b) Ni_3Fe, (c) Ni_3FeN and (d) Ni_3FeN/Ni_3Fe-bulk at various scan rates (40, 60, 80 ,100 and 120 mV s^{-1}) in 1.0 M KOH for HER.

Fig. S13 LSV curves normalized to the electrochemically active surface area (ECSA) for (a) OER and (b) HER.

Fig. S14 (a) LSV curves and (b) Tafel plots for OER evaluation of samples derived from Ni_3FeAl-LDH precursors with different ratios of Fe^{3+}: Al^{3+} (10: 0, 9.5: 0.5, 9: 1, 8: 2 and 7: 3). (c) LSV curves and (d) Tafel plots for HER evaluation of samples derived from Ni_3FeAl-LDH precursors with different ratios of Fe^{3+}: Al^{3+} (10: 0, 9.5: 0.5, 9: 1, 8: 2 and 7: 3).

Fig. S15 (a) LSV curves and (b) Tafel plots for OER evaluation of d-Ni_3FeN/Ni_3Fe with different thermal ammonolysis temperature (400℃, 450℃, 500℃, 550℃ and 600℃). (c) LSV curves and (d) Tafel plots for HER evaluation of d-Ni_3FeN/Ni_3Fe with different thermal ammonolysis temperature (400℃, 450℃, 500℃, 550℃ and 600℃).

Table S1. Comparison of OER performance in alkaline medium for d-Ni_3FeN/Ni_3Fe with other recently reported OER electrocatalysts.

Table S2. Comparison of HER performance in alkaline medium for d-Ni_3FeN/Ni_3Fe with other recently reported HER electrocatalysts.

Table S3. Comparison of two-electrode overall water splitting performance in alkaline medium for d-Ni_3FeN/Ni_3Fe with other recently reported electrocatalysts.

Table S4 Comparison of the value of C_{dl}, R_s, R_{ct} for different catalyst samples for OER in alkaline medium.

Table S5 Comparison of the value of C_{dl}, R_s, R_{ct} for different catalyst samples for HER in alkaline medium.

Chemicals

$Al(NO_3)_3 \cdot 9H_2O$ (MW: 375.13) and NaOH were purchased from Sinopharm Chemical Reagent Co., Ltd. $Fe(NO_3)_3 \cdot 9H_2O$ (MW: 404), $NaNO_3$ and Formamide were obtained from MACKLIN Co., Ltd. $Ni(NO_3)_2 \cdot 6H_2O$ (MW: 290.79), Nafion (5 wt%), commercial Pt/C (20 wt%) catalyst and commercial IrO_2 catalyst were ordered at Sigma-Aldrich Co. Ltd. All of the reagents were purchased and directly used without further purification.

Synthesis Method

Synthesis of Ni_3FeN: The synthesis procedure is very similar with that of d-Ni_3FeN/Ni_3Fe. Firstly, solution A containing of 1.50 mmol

$Ni(NO_3)_2 \cdot 6H_2O$ and 0.50 mmol $Fe(NO_3)_3 \cdot 9H_2O$ (Ni/Fe molar ratios was 30:10) were dissolved in 40.0 mL of distilled water. Solution B containing $NaNO_3$ was prepared by dissolving the salt in 40 mL distilled water containing 25 vol% formamide to give a base concentration of 0.020 M. Solution A was added to solution B drop by drop. Simultaneously, 100 ml 0.25 M NaOH was added dropwise to solution B to maintain the system at a pH value of ca. 10 under magnetic stirring at 80 ° C. The reaction was completed within 30 min. The precipitates were collected by centrifugation, washed with water and ethanol for 3 times, respectively, and then freeze-dried for 12h to prepare ultrathin Ni_3Fe-LDH nanosheets. Finally, Ni_3Fe-LDH nanosheets were pyrolyzed by heating to 500 ° C at a heating rate of 5 ° C min^{-1} under a NH_3 gas flow and further treated at 500 ° C under NH_3 for 2 h. After the temperature had reduced to room temperature naturally, Ni_3FeN nanosheets were synthesized.

Synthesis of Ni_3Fe: The synthesis method of Ni_3Fe is very similar to that of d-Ni_3FeN/Ni_3Fe. The only difference is Ni_3Fe was obtained after pyrolyzing under H_2/Ar flow instead of NH_3 flow, and the rest synthesis process was same as d-Ni_3FeN/Ni_3Fe.

Synthesis of Ni_3FeN/Ni_3Fe-bulk: Ni_3FeN/Ni_3Fe-bulk was synthesized through hydrothermal method. 6.0 mmol $Ni(NO_3)_2 \cdot 6H_2O$ (1.74 g), 2.0 mmol $Fe(NO_3)_3 \cdot 9H_2O$ (0.808 g), 40.0 mmol urea (2.40 g) and 16.2 mmol NH_4F (0.60 g) were dissolved in 80 mL H_2O, and then transferred to a Teflon-lined autoclave at 120 ° C for 25 h. After the same above-mentioned thermal ammonolysis process, the Ni_3FeN/Ni_3Fe-bulk was fabricated.

Materials characterization

The morphology and composition of the materials were characterized by SEM, TEM, AFM, XRD, XPS, XANES and EXAFS measurements. A JSM-7500F field-emission scanning electron microscope was used to record SEM images. TEM and HRTEM images were collected on a JEOL JEM-2100F transmission electron microscope with an operating voltage of 200 kV. AFM images were investigated by a Multimode 8 SPM 9700 atomic force microscope. XRD was obtained on a D/Max2000 X-ray diffraction system. XPS spectra were recorded on an Escalab instrument (Escalab 250 xi, Thermo scientific, England) with a calibration relative to the carbon 1s standard value of 284.6 eV. Ni and Fe K-edge XANES and EXAFS spectra were tested by the BL10C beam line with the Pohan Light Source (PLS-II)

Electrochemically active surface area (ECSA) calculation

In this work, we use electrochemical double layer capacitances (C_{dl}) to characterize electrochemical active surface area (ECSA). The C_{dl} was measured by cyclic voltammograms in a potential region of 0 V to 0.2 V vs RHE with different scan rate of 40 to 120 mv s^{-1}. The C_{dl} is estimated by plotting the ΔJ $(J_a-J_c)/2$ at 0.1 V vs. RHE against the scan rates, where the slope is C_{dl}. The ECSA of 1 cm^2 is represented by a special capacitance value (C_s) 0.040 mF cm^{-2} in 1 M KOH based on typical reported values. Hence, the ECSA of the catalyst layer can be calculated as:

$$ECSA = \frac{C_{dl}}{C_s}$$

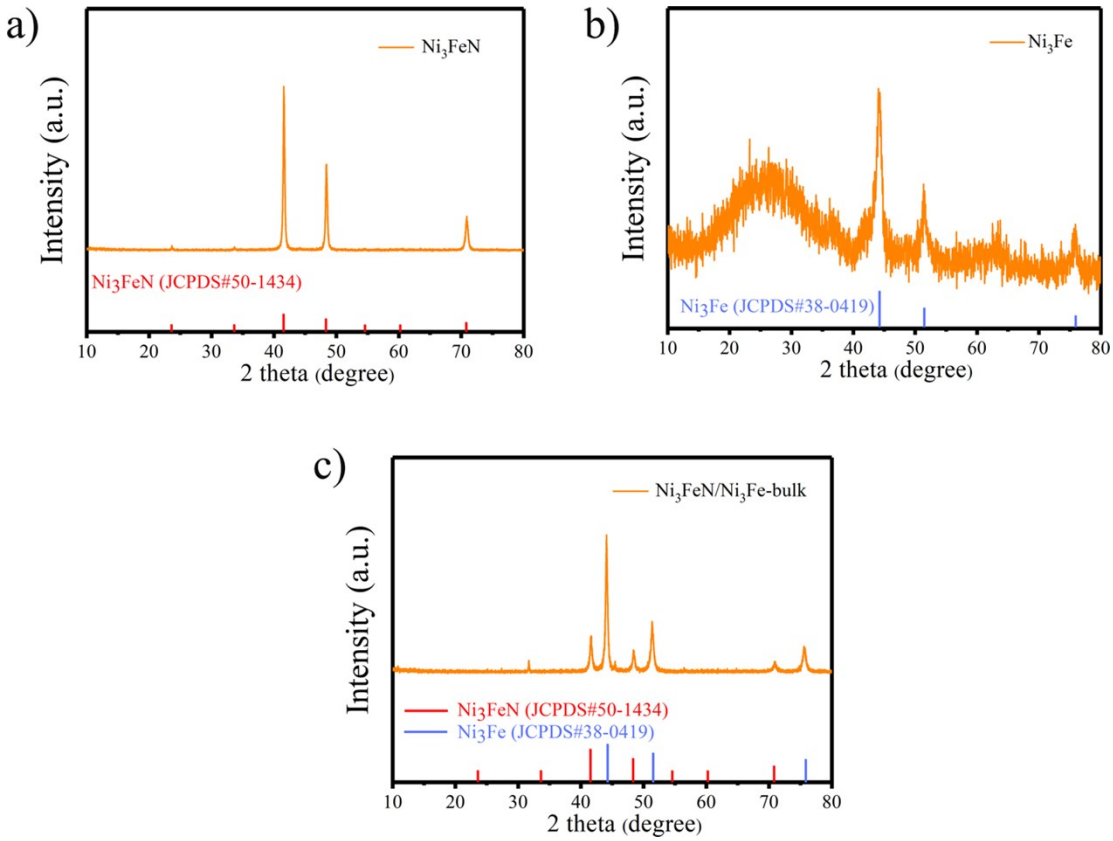

Fig. S1 XRD patterns of (a) Ni_3FeN, (b) Ni_3Fe and (c) Ni_3FeN/Ni_3Fe-bulk.

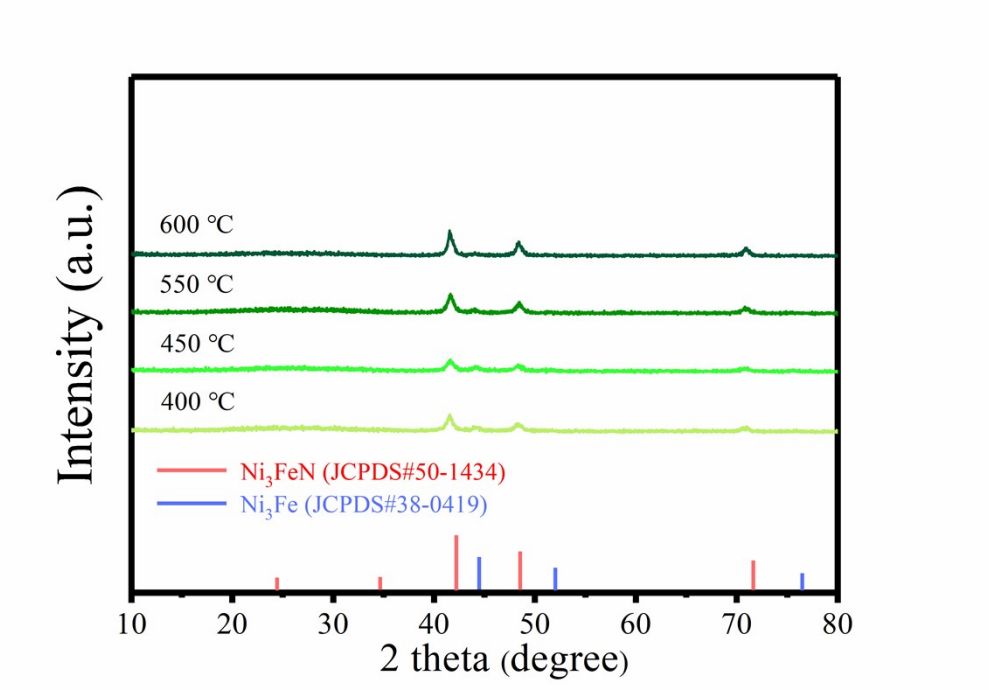

Fig. S2 XRD patterns of d-Ni_3FeN/Ni_3Fe with different thermal ammonolysis

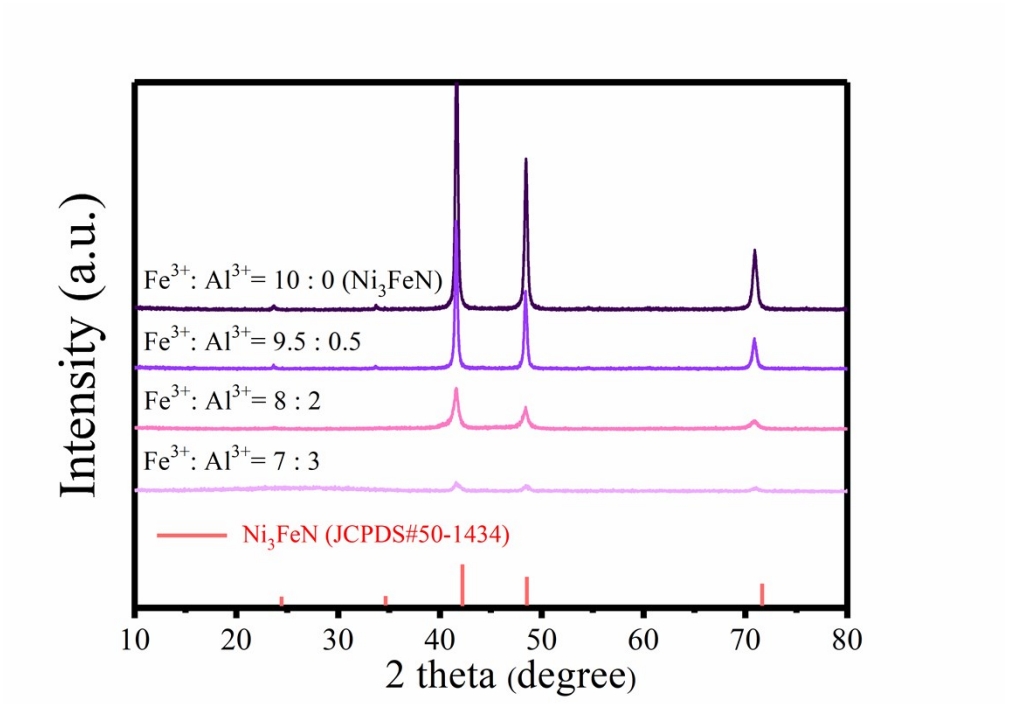

Fig. S3 XRD patterns of samples derived from other Ni_3FeAl-LDH precursors

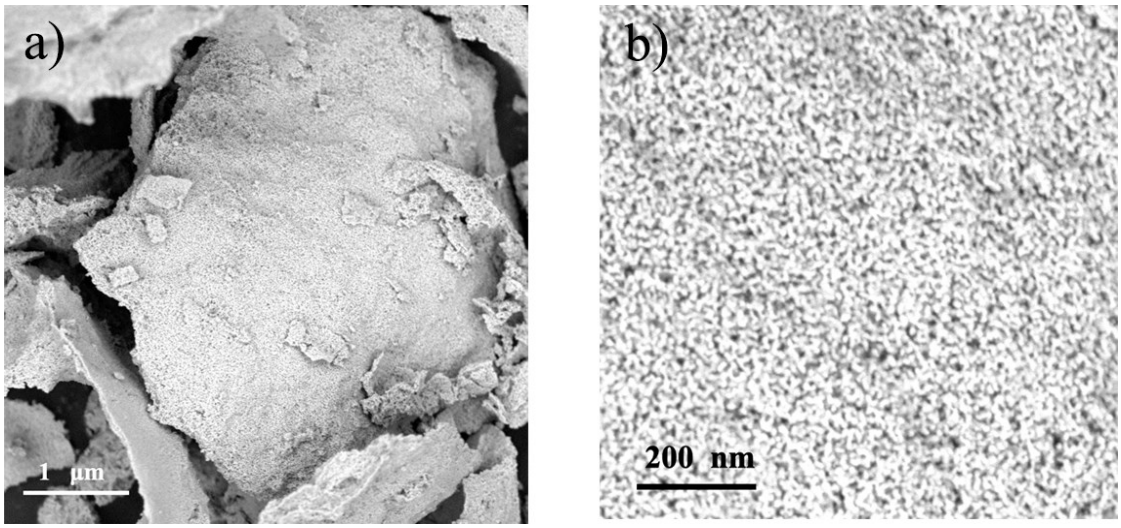

Fig. S4 (a) low-magnification SEM and (b) SEM images of d-Ni_3FeN/Ni_3Fe.

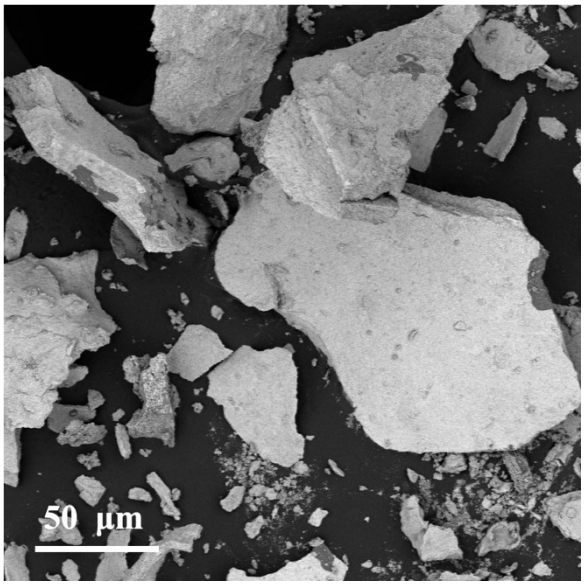

Fig. S5 SEM image of Ni_3FeN/Ni_3Fe-bulk.

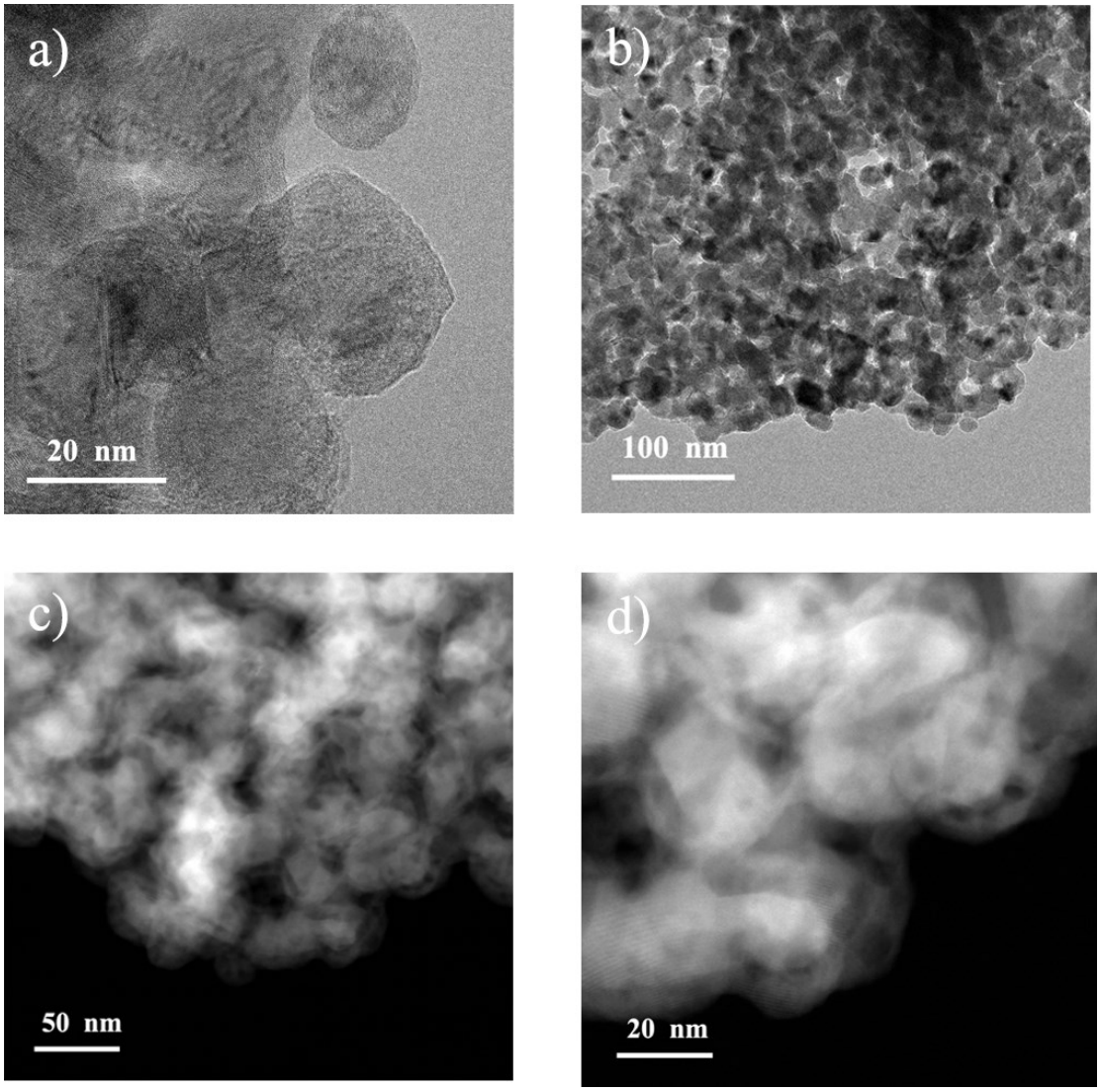

Fig. S6 (a) low-magnification TEM and (b) TEM images of d-Ni_3FeN/Ni_3Fe. (c-d) HAADF-STEM images of d-Ni_3FeN/Ni_3Fe.

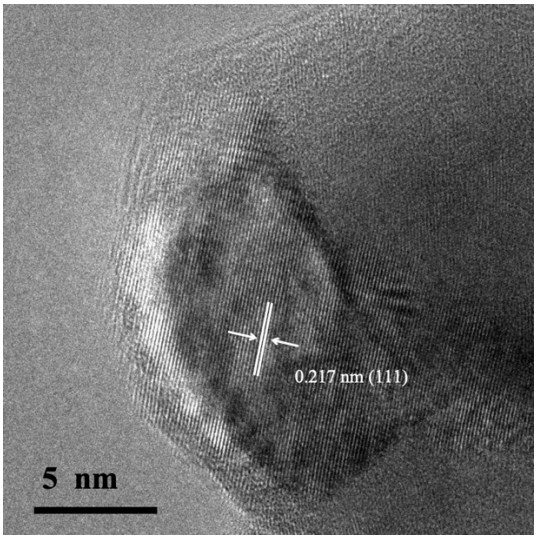

Fig. S7 HRTEM image of Ni_3FeN.

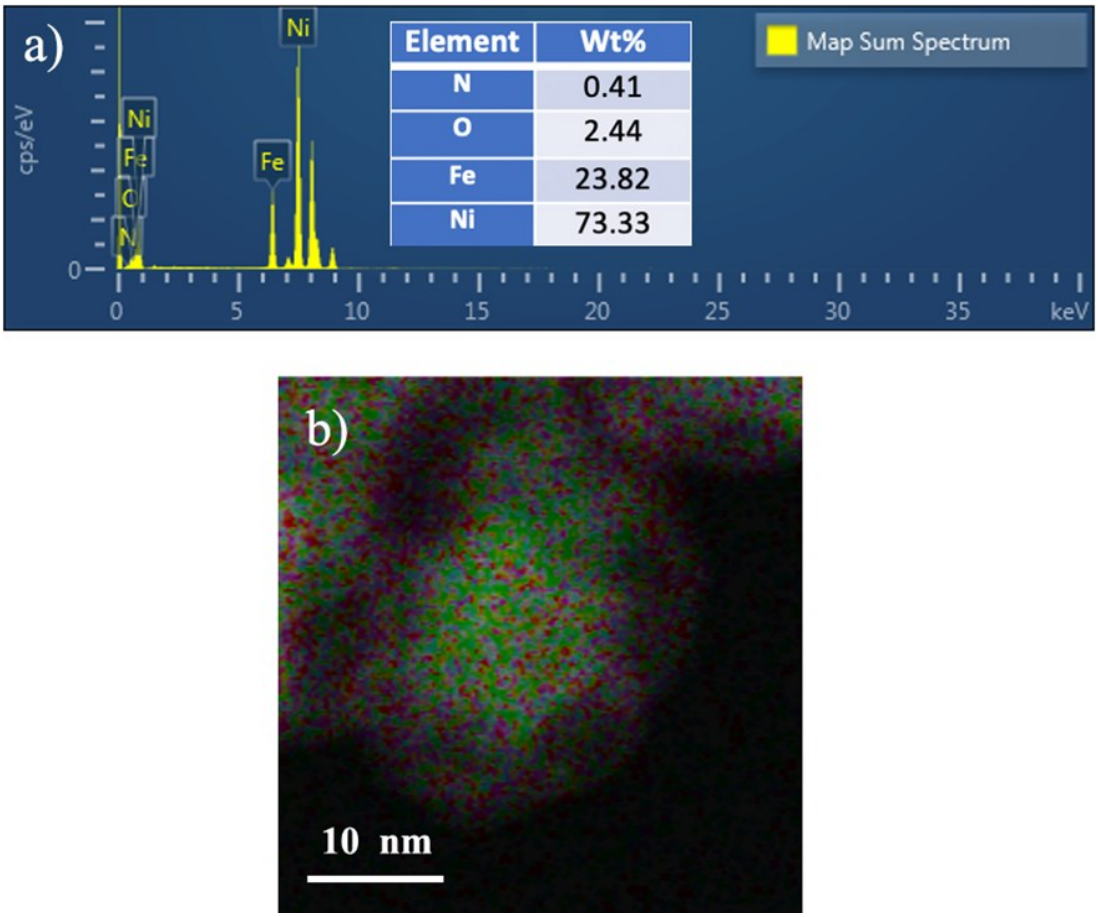

Fig. S8 (a) EDX spectrum of d-Ni_3FeN/Ni_3Fe. (b) Elemental distribution mapping of d-Ni_3FeN/Ni_3Fe.

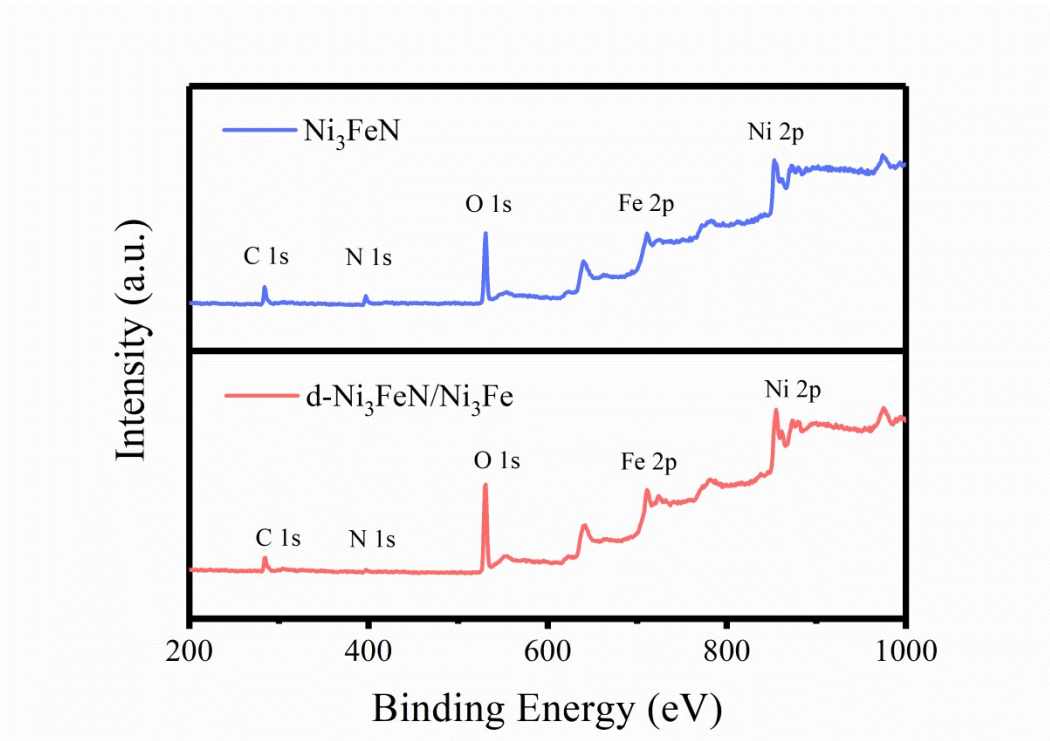

Fig. S9 XPS survey spectra of Ni_3FeN and d-Ni_3FeN/Ni_3Fe (top: Ni_3FeN, bottom: d-Ni_3FeN/Ni_3Fe).

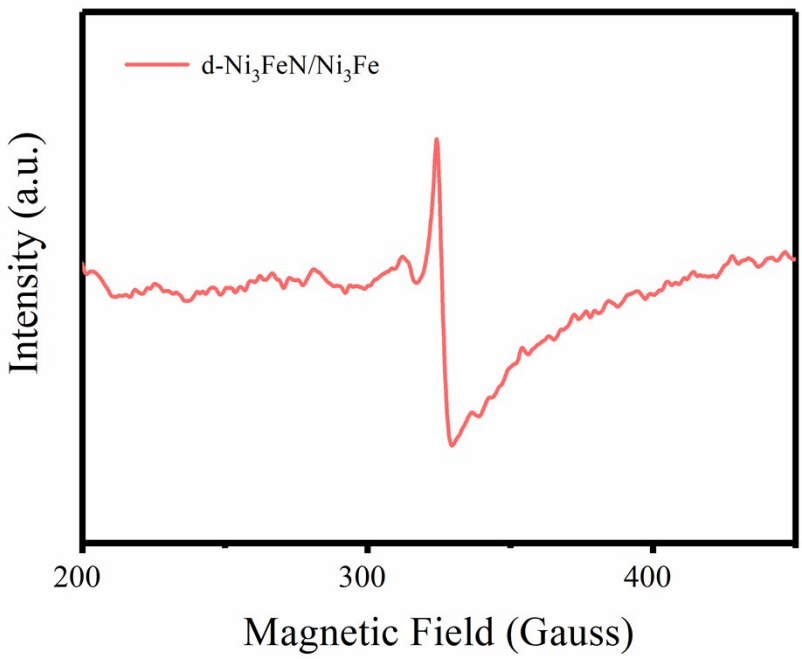

Fig. S10 EPR spectrum of d-Ni_3FeN/Ni_3Fe.

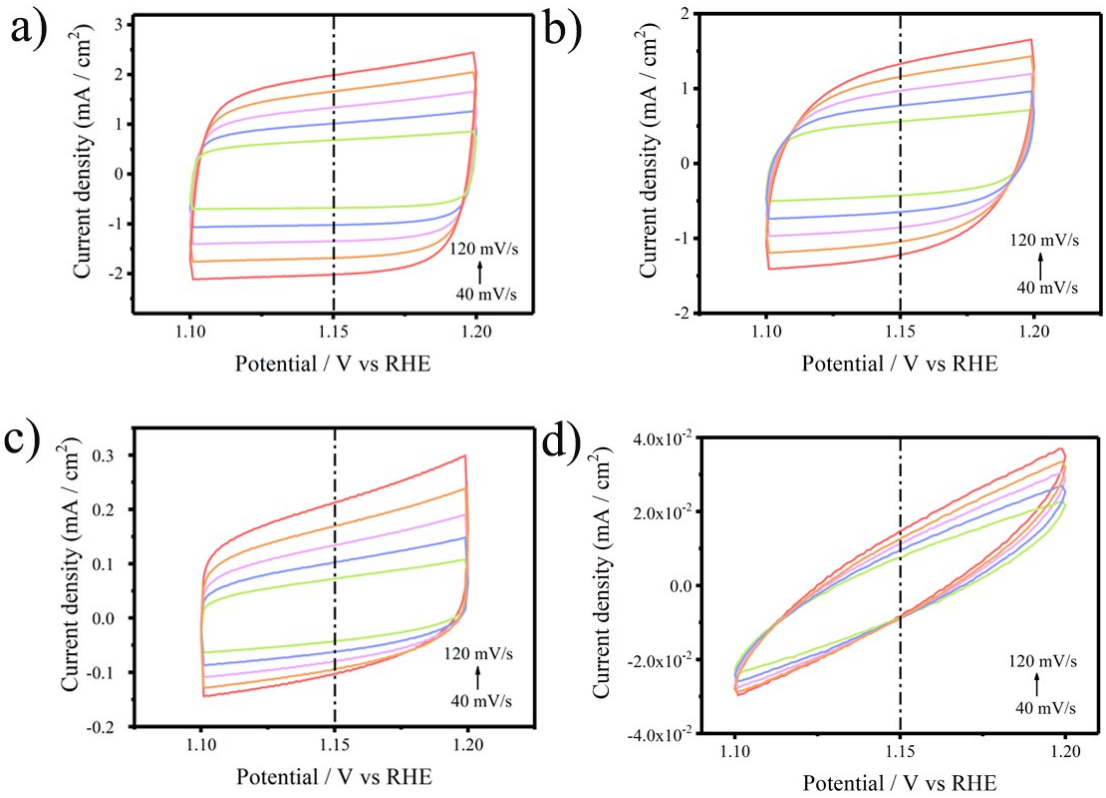

Fig. S11 Cyclic voltammetry curves of the (a) d-Ni_3FeN/Ni_3Fe, (b) Ni_3Fe, (c) Ni_3FeN and (d) Ni_3FeN/Ni_3Fe-bulk at various scan rates (40, 60, 80 ,100 and 120 mV s^{-1}) in 1.0 M KOH for OER.

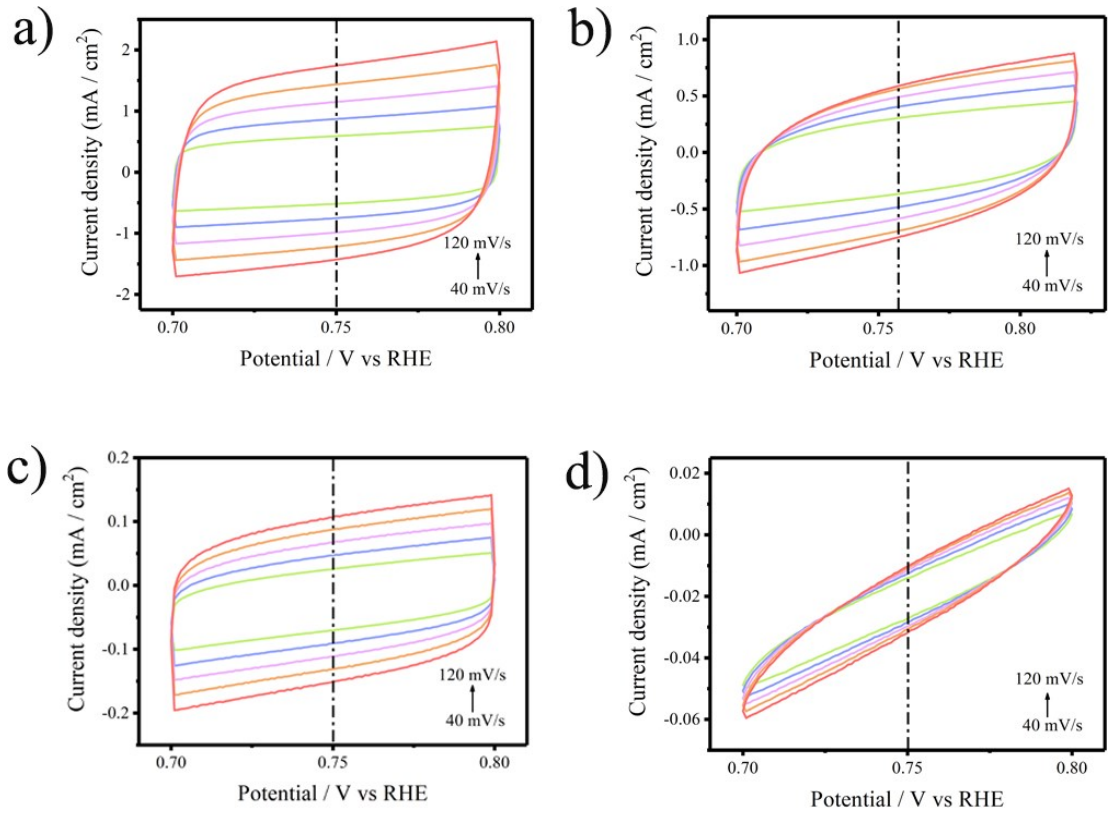

Fig. S12 Cyclic voltammetry curves of the (a) d-Ni_3FeN/Ni_3Fe, (b) Ni_3Fe, (c) Ni_3FeN and (d) Ni_3FeN/Ni_3Fe-bulk at various scan rates (40, 60, 80 ,100 and 120 mV s^{-1}) in 1.0 M KOH for HER.

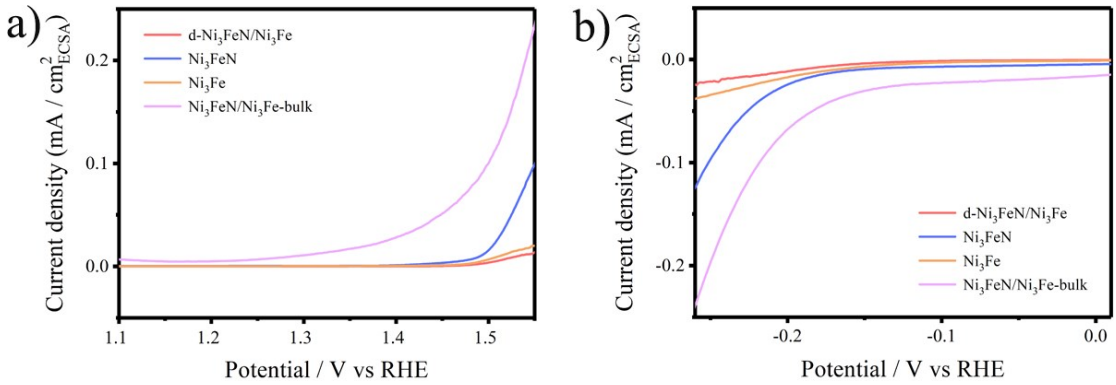

Fig. S13 LSV curves normalized to the electrochemically active surface area (ECSA) for (a) OER and (b) HER.

We normalized the LSV curves by ECSA calculated from C_{dl}. However, in fact, the results shown below were not ideal. We believed that due to the d-Ni_3FeN/Ni_3Fe's ultrathin nanosheet morphology and large amount of lattice defects, the ECSA value of d-Ni_3FeN/Ni_3Fe for OER and HER significantly increased, which was much bigger than Ni_3FeN, Ni_3Fe and Ni_3FeN/Ni_3Fe-bulk. Therefore, the specific activity of d-Ni_3FeN/Ni_3Fe was smaller than other samples.

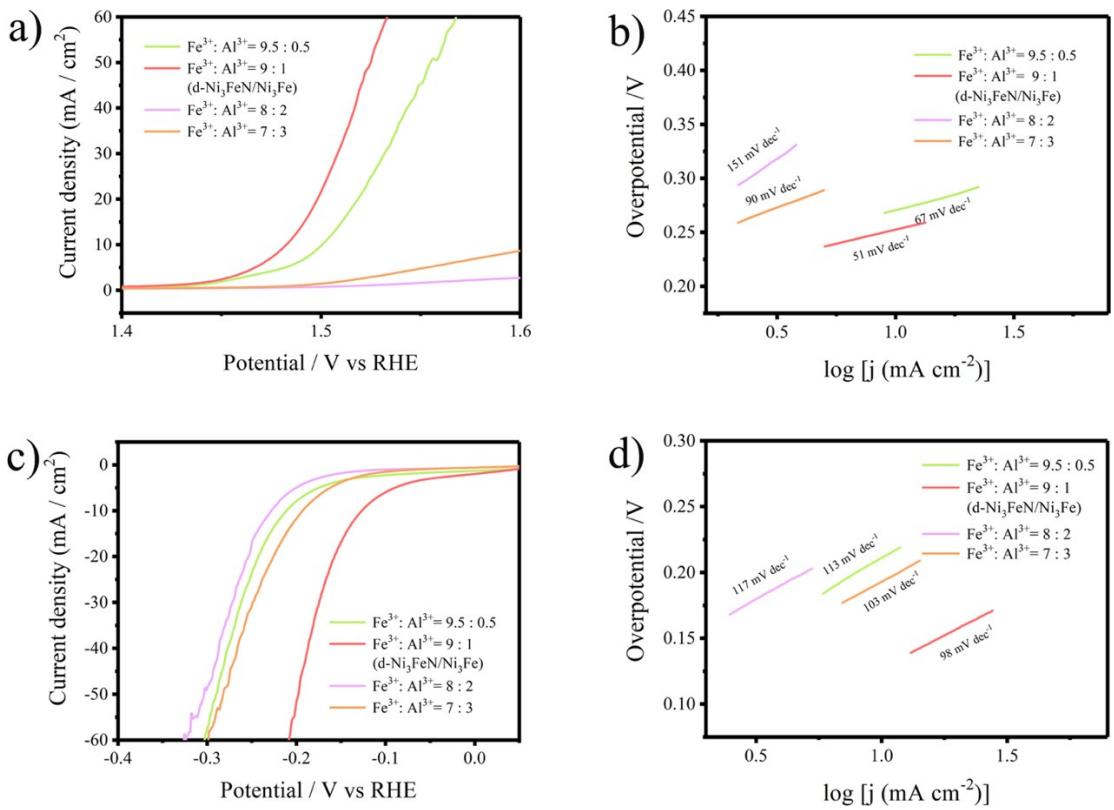

Fig. S14 (a) LSV curves and (b) Tafel plots for OER evaluation of samples derived from Ni_3FeAl-LDH precursors with different ratios of Fe^{3+}: Al^{3+} (9.5: 0.5, 9: 1, 8: 2 and 7: 3). (c) LSV curves and (d) Tafel plots for HER

In order to better illustrate the effect of defect density on catalytic performances, using the same synthesis method, we supplemented a series of Ni_3Fe-LDH-V_{Al} precursors with different Al vacancies by varying the Fe^{3+}/Al^{3+} molar ratio (9.5: 0.5, 9: 1, 8: 2 and 7: 3), and annealed them with the same procedure, thus obtaining a series of d-Ni_3FeN/Ni_3Fe with different defect density. The OER and HER activities were tested under the same conditions and shown in Fig. S13. Apparently, the electrocatalytic activity first increases as the amount of Al vacancies increases, as demonstrated by the superior OER and HER activities of 9: 1 to 9.5: 0.5. This can be attributed to the increase of defects, which leads to the increase of active sites on d-Ni_3FeN/Ni_3Fe. However, with the further increase of Al vacancies, the catalytic activity shows obvious decay, owing to that abundant defects on d-Ni_3FeN/Ni_3Fe contribute to the decrease of interfacial area volume, destruction of both the optimized electron state and integrity of the structure.

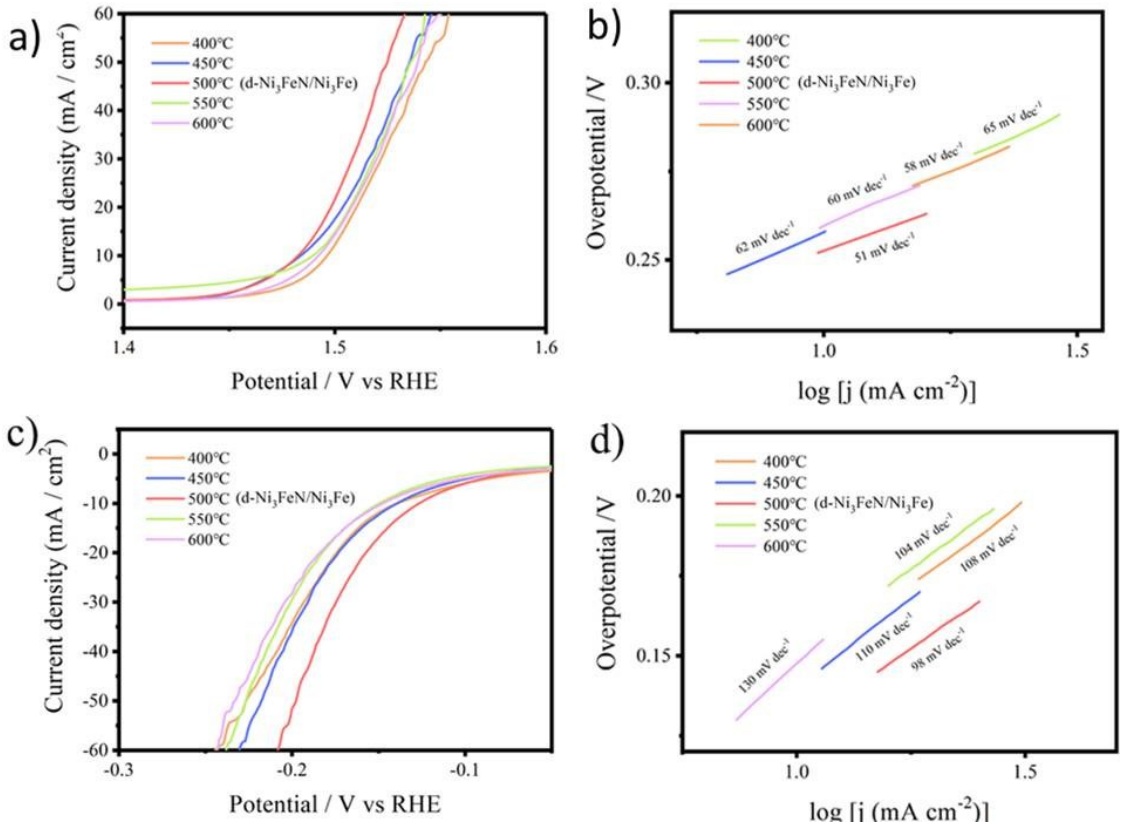

Fig. S15 (a) LSV curves and (b) Tafel plots for OER evaluation of d-Ni_3FeN/Ni_3Fe with different thermal ammonolysis temperature (400℃, 450℃, 500℃, 550℃ and 600℃). (c) LSV curves and (d) Tafel plots for HER evaluation of d-Ni_3FeN/Ni_3Fe with different thermal ammonolysis temperature (400℃, 450℃, 500℃, 550℃ and

Table S1 Comparison of OER performance in alkaline medium for d-Ni_3FeN/Ni_3Fe with other recently reported OER electrocatalysts.

Catalyst	Overpotential (10 mA cm^{-2})	Tafel slop (mV dec^{-1})	Electrolyte	Ref.
d-Ni_3FeN/Ni_3Fe	250	51	1 M KOH	This work
CM (1:0.1)	300	118	1 M KOH	Sci. Bull. **2020**, *65*, 460-466
MoS_2/*r*Fe-$NiCo_2O_4$	270	39	1 M NaOH	J. Am. Chem. Soc. **2020**, *142*, 50-54
$Co_{0.15}Fe_{0.85}N_{0.5}$ NSs	266	30	1 M KOH	Nano Energy. **2019**, *57*, 644-652
$Fe_{7.2\%}$-Ni_3S_2 NSs/ NF	295	71	1 M KOH	Nanoscale, **2019**, *11*, 2355-2365
$Mo_{51}Ni_{40}Fe_9$ NBs	257	51	1 M KOH	ACS Catal. **2019**, *9*, 1013−1018
Fe_1Ni_2-BDC	260	35	1 M KOH	ACS Energy Lett. **2019**, *4*, 285−292
$Co_{0.5}(V_{0.5})$	282	64	1 M KOH	Adv. Energy Mater. **2019**,*10*, 1903571
W_2N/WC	320	83.8	1 M KOH	Adv. Mater. **2019**, *32*, 1905679
Co_3O_4/CeO_2 NHs	270	60	1 M KOH	Adv. Mater. **2019**, *31*, 1900062
Fe-UTN	270	36.6	1 M KOH	Angew. Chem. Int. Ed. **2019**, *59*, 2313-2317

Table S2 Comparison of HER performance in alkaline medium for d-Ni_3FeN/Ni_3Fe with other recently reported HER electrocatalysts.

Catalyst	Overpotential (10 mA cm^{-2})	Tafel slop (mV dec^{-1})	Electrolyte	Ref.
d-Ni_3FeN/Ni_3Fe	125	98	1 M KOH	This work
Fe_3C-Co/NC	238	108.8	1 M KOH	Adv. Funct. Mater. **2019**, *29*, 1901949
O-Co_2P-3	160	61.1	1 M KOH	Adv. Mater. **2017**, *29*, 1606980
$Fe_2P_2S_6$ NCs	175	137	1 M KOH	Small Methods **2019**, *4*, 19006323
R-NCO	135	52	1 M KOH	J. Am. Chem. Soc. **2018**, *140*, 13644−13653
Co-Ni_3N	194	156	1 M KOH	Adv. Mater. **2018**, *30*, 170551
Crys-AMO	138	50	1 M KOH	J. Mater. Chem. A, **2019**, *7*, 257–268
Co-MoS_2	179	62	1 M KOH	ACS Nano **2018**, *12*, 4565−4573
Co-BDC/MoS_2	248	86	1 M KOH	Small **2019**, *15*, 1805511
NiFeP	178	69	1 M KOH	Appl. Surf. Sci. **2018**, *457*, 1081–1086
PN-CMS40 NTs	178	98	1 M KOH	J. Mater. Chem. A, **2017**, *5*, 25410–25419

Table S3 Comparison of two-electrode overall water splitting performance in alkaline medium for d-Ni_3FeN/Ni_3Fe with other recently reported electrocatalysts.

Catalyst	Voltage (10 mA cm^{-2})	Electrolyte	Ref.
d-Ni_3FeN/Ni_3Fe	1.61	1 M KOH	This work
Co2P/CoP	1.65	1 M KOH	J. Power Sources. **2018**, *402*, 345
Co-NC@Mo_2C	1.685	1 M KOH	Nano Energy. **2019**, *57*, 746-752
NF@G-5@Ni_3S_2	1.62	1 M KOH	J. Electroanal. Chem, **2020**, *858*, 113795
Ni/Ni(OH)$_2$	1.59	1 M KOH	Adv. Mater. **2020**, *32*, 1906915
MoS_2-NiS_2/NGF/NF	1.64	1 M KOH	Appl. Catal. B. **2019**, *254*, 15–25
E-Mo–NiCoP	1.61	1 M KOH	Nano-Micro Lett. **2019**, 11:55
CoFeZr oxides/NF	1.64	1 M KOH	Adv. Mater. **2019**, *31*, 1901439
P–Co_3O_4 NWs	1.61	1 M KOH	Energy Stor. Mater. **2019**, *23*, 1-7
CoP NFs	1.65	1 M KOH	ACS Catal. **2020**, *10*, 412−419

Table S4 Comparison of the value of C_{dl}, R_s, R_{ct} for different catalyst samples for OER in alkaline medium.

Catalyst Sample	C_{dl} (F)	R_s (Ω)	R_{ct} (Ω)
d-Ni_3FeN/Ni_3Fe	0.00091	13.41	35.58
Ni_3FeN	0.00052	9.65	55.89
Ni_3Fe	0.00484	10.35	51.78
Ni_3FeN/Ni_3Fe-bulk	0.00003	11.22	1381.23
IrO_2	0.00043	13.48	40.94

Table S5 Comparison of the value of C_{dl}, R_s, R_{ct} for different catalyst samples for HER in alkaline medium.

Catalyst Sample	C_{dl} (F)	R_s (Ω)	R_{ct} (Ω)
d-Ni_3FeN/Ni_3Fe	0.00058	16.91	32.56
Ni_3FeN	0.00052	11.54	56.77
Ni_3Fe	0.00102	10.35	51.78
Ni_3FeN/Ni_3Fe-bulk	0.00005	10.21	1386.94
Pt/C	0.00027	10.18	31.76